NUMERICAL INVESTIGATION OF STEADY STATE THERMAL BEHAVIOR OF AN INFRARED DETECTOR CRYOCHAMBER

Mayank Singhal, Gaurav Singhal[#,*], Avinash C. Verma[#], Sushil Kumar, Manmohan Singh

Solid State Physics laboratory, Timarpur, Delhi -11054
[#]Laser Science and Technology Centre, Metcalfe House, Delhi -110054

An infrared (IR) detector is simply a transducer of radiant energy, converting radiant energy in the infrared into a measurable form. Since infrared radiation does not rely on visible light, it offers the possibility of seeing in the dark or through obscured conditions, by detecting the infrared energy emitted by objects. One of the prime applications of IR detector systems for military use is in target acquisition and tracking of projectile systems. IR detectors also have great potential in commercial market. Typically, infrared detectors perform best when cooled to cryogenic temperatures in the range of nearly 120 K. However, the necessity to operate in such cryogenic regimes makes the application of IR detectors extremely complex. Further, prior to proceeding on to a full blown transient thermal analysis it is worthwhile to perform a steady state numerical analysis for ascertaining the effect of variation in viz., material, gas conduction coefficient (h), emissivity (ε) on the temperature profile along the cryochamber length. This would enable understanding the interaction between the cryochamber and its environment. Hence, the present work focuses on the development of steady state numerical models for thermal analysis of IR cryochamber using MATLAB. The numerical results show that gas conduction coefficient has marked influence on the temperature profile of the cryochamber whereas the emissivity has a weak effect. The experimental validation of numerical results has also been presented.

Key words: Infrared detector, Cryochamber, Gaseous conduction, Thermal analysis

1.0 Introduction

The application of thermal sciences is not only limited to common engineering scenarios but is being potentially extended to realms which have not been envisaged earlier. One such modern application, which has come to the fore, is in the analysis and prediction of thermal behavior of infrared (IR) detector cryochamber. Infrared detectors are devices, which are highly sensitive to temperature and require special cryochambers, maintained under high vacuum, for housing them for their optimal functioning.

[*]Corresponding author, email: singhal_g@rediffmail.com

Infrared (IR) detectors have been called the *eyes of the digital battlefield.* In general, military applications have spearheaded and dominated the requirements in this field akin to many other emerging fields. One of the prime applications of IR detector systems for military use is in target acquisition and tracking of projectile systems [1]. IR detectors also have great potential in commercial market with the market share expected to grow by over 70% in volume and 40% in value [2]. Non-military uses of IR detector systems include thermal efficiency analysis, remote temperature sensing, short-ranged wireless communication, spectroscopy, and weather forecasting.

In general, only scant amount of data [3-5] regarding thermal analysis of IR devices is available in open literature more so because of classified nature of its applications. An experimental study by Kang et.al [3] and an analytical study for steady state cooling have been reported by Kim et.al [4]. Another experimental study by Kim et.al [5] investigating cryochamber operation at pressureôs in the region of 10^{-3} torr or below has been reported.

However, detailed works attempting rigorous thermal modeling of cryochamber detector assembly are still lacking. The thrust of the paper, therefore, is to present a steady state numerical analysis of cryochamber detector assembly taking into account all heat loads in their original form.

2.0 Numerical Simulation

The investigation of cooling characteristic of an infrared detector cryochamber is actually a relatively complex heat transfer problem. This occurs primarily because of the kind of heat transfer processes involved in the analysis. In a cryochamber, conduction and radiation occur simultaneously and both steady and transient responses are important. Due to these seemingly complex heat transfer processes, very few modeling efforts [4] have been undertaken till date.

This section deals with the modeling of heat transfer processes and the analysis of effect of variation of parameters on temperature profile of cryochamber in steady state operating mode.

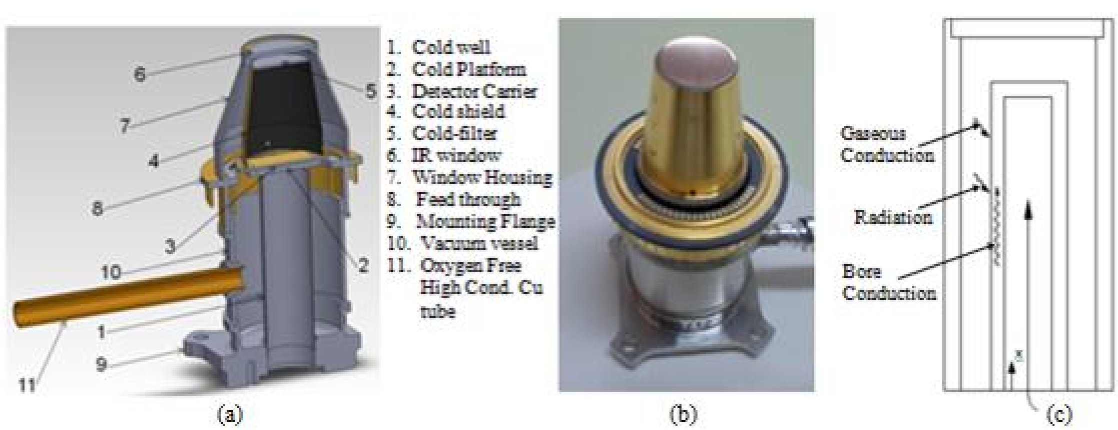

Fig. 1: Typical cryochamber; (a) Solid works view (b) Hardware (c) Modes of heat transfer

The thermal modeling for a generalized cryochamber domain has been carried out using the typical configuration shown in fig. 1, which also shows the solid works view and typical hardware

Basically, the cryochamber has the following components viz., i) vacuum vessel (outer cylinder), ii) a cold well (inner axi-symmetric thin walled structure), and iii) a feed through unit, iv) IR detector is located on the top of the cold well, v) IR window i.e. the roof of the cylinder through which the detector receives the signal. The vacuum vessel is made of stainless steel material, whereas the cold finger is a thin cylindrical vessel made of glass or steel. It is evident that the thickness in case of glass will be greater than in steel on account of its mechanical integrity. The base is again made of stainless steel.

The space between the vacuum vessel and the cold well is maintained under vacuum to minimize heat loss by evacuation through a pump. The cold well shape is mostly cylindrical and the cooling is executed by an external cooler, which may be based on various refrigeration schemes (Stirling, Joule – Thompson etc).

In order to correctly solve the problem the foremost objective is to ascertain the possible modes of heat transfer. Simultaneously, it is also essential to identify those possible modes of heat transfer whose contribution is negligible. In the final analysis these latter modes of heat transfer will be neglected greatly simplifying the problem to obtain realistic results. The possible modes of heat transfer in the present case are;

i) Heat conducted from the base to the top of the cold well along the thin wall
ii) Radiative heat transfer occurs between the inner surface of the vacuum vessel and outer surface of the cold well.
iii) Natural convection on to the cold well
iv) Although, domain is under vacuum, however, the remaining gas may participate in heat transfer on account of gaseous conduction.

Here, it is pertinent to mention that heat load due to natural convection, designated as (iii) may be neglected. The reason is that due to small domain dimension, the Nusselt number (Nu) determined on the basis of gap spacing for the given annular interior space (solved as a vertical large aspect ratio enclosure) is small [6]. Moreover, the Rayleigh number (Ra= Pr*$g\Delta T\delta^3/T_{avg}\nu^2$), is much smaller (~1) than critical Rayleigh number ($Ra_{crtical}$) owing to small annular spacing, δ (~5 mm) and high kinematic viscosity (3.3 x 10^{-3} m^2s^{-1}) at low T and P negating the onset of natural convection due to Rayleigh- Bernard instability. This is because the $Ra_{crtical}$ is required to be; > 657 [7] for free boundaries, > 1100 [8] for rigid- free case and for rigid – rigid geometry > 1708 [9] (present case). Further, gas conduction is dealt using a coefficient (*h*) units of $Wm^{-2}K^{-1}$ [6, 10], apparently because $k/L \sim h$ (are of the same order).

Assumption

i) Heat transfer due to convection may be neglected.
ii) Since the cold well is a thin cylinder (typical thicknesses close to 1mm), the conduction may be considered to be one dimensional i.e. along the axis. If one were to calculate the Biot number, it would turn out be of the order of 0.02, indicating that transverse gradients are negligible.
iii) The cold well finger inserted into the bore has the same temperature distribution as the cold well, thus neglecting heat transfer analysis at the internal surface of the cold well.
iv) The thermal contact resistance between the metal (stainless steel) base and the glass bore is negligible since the glass is typically fused to be bond to the base. Therefore, "T_b" is the same as the temperature of the metal base, which is identical to the ambient temperature "T_∞".

v) At the other end detector array is bonded to the glass bore by an epoxy and it is assumed the temperature of the end of glass bore is same as the detector *(T_d)*.

vi) The shape factor, which in the present case is the fraction of energy leaving the vacuum vessel and intercepted by the cold well, for radiation heat transfer is unity.

The thermal modeling of the cryochamber has been carried out for steady state case. The basic energy balance for an elemental volume of the cold well in case of steady state heat transfer is shown in fig. 2.

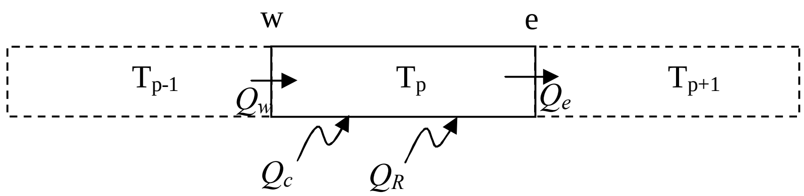

Fig. 2: Heat transfer in an elemental volume of cold well

Hence, this can be mathematically represented as,

$$Q_w + Q_c + Q_R = Q_e \qquad \textbf{(1)}$$

The terms *'Q_w'* and *'Q_e'* represent the heat being conducted into the finite volume and away from it and can be expressed using the Fourierôs law. *'Q_c'* represents the term because of *gaseous conduction* and is expressed as function of heat transfer coefficient, temperature difference and the circumferential area of the finite volume under consideration. *'Q_R'* represents the radiative heat transfer which is mathematically expressed by means of the Stefan Boltzmann law. Thus, eq. (1) may be transformed as in eq. (2),

$$-kA(dT/dx) + P\delta x h(T_a - T_p) + P\delta x \sigma\varepsilon(T_a^4 - T_p{}^4) = -kA(dT/dx) + \frac{d}{dx}(-kA\frac{dT}{dx})\delta x \qquad \textbf{(2)}$$

Further, simplifying the equation we get,

$$kA\frac{d^2T}{dx^2} + Ph(T_a - T_p) + \sigma.P\varepsilon(T_a^4 - T_p{}^4) = 0 \qquad \textbf{(3)}$$

Eq. (3) can further be modified as,

$$\frac{d^2T}{dx^2} + \frac{Ph}{kA}(T_a - T_p) + \frac{\sigma.P.\varepsilon}{kA}(T_a^4 - T_p{}^4) = 0 \qquad \textbf{(4)}$$

In order to solve the problem numerically, eq. (4) is to be integrated over the finite volume from control surface *w'* to control surface *'e'*. Thus, eq. (4) may be expressed as,

$$\int_w^e \frac{d^2T}{dx^2}dx + \int_w^e \frac{Ph}{kA}(T_a - T_p)dx + \int_w^e \frac{\sigma.P\varepsilon}{kA}(T_a^4 - T_p{}^4)dx = 0 \qquad \textbf{(5)}$$

Term (I) **Term (II)** **Term (III)**

Term (I) and term (II) can be expressed for discretization quite easily. Hence, eq. (5) may be written as,

$$\left(\left.\frac{dT}{dx}\right|_e - \left.\frac{dT}{dx}\right|_w\right) + \frac{Ph}{kA}(T_a - T_P)\Delta x + \frac{\sigma.P\varepsilon}{kA}T_a^4.\Delta x - \int_w^e \frac{\sigma.P}{kA}\varepsilon T^4 dx = 0 \tag{6}$$

However, a part of the term (III) is non linear term as is clearly evident in eq. (6) with finite volume representative temperature appearing as a power of ó4ô. Hence, it needs to be linearized. The linearization procedure adopted is as suggested by Patankar [11].

The last term of eq. (6) i.e. $\int_w^e \frac{\sigma.P}{kA}\varepsilon T^4 dx$ may be treated as a source term (S) and expressed as,

$$S = S_c + S_p T_p = S^* + \left(\frac{dS}{dT}\right)^* (T - T^*) \tag{7}$$

Here ó*ô values represent previous iteration values of the variable being sought, which in this case is *'T_p'*. As will be evident later when we discuss the operating algorithm, the solution of the eq. (5) would require iteration for non ï linearity. The terms *'S_c'* and *'S_p'* turn out to be,

$$S_c = -3.\frac{\sigma.P}{kA}.\varepsilon.T_p^{*4}$$

$$S_p = 4\frac{\sigma.P}{kA}.\varepsilon.T_p^{*}$$

Thus, eq. (6) on discretization may be written as,

$$\left[\frac{T_{P+1} - 2T_P + T_{P-1}}{\Delta x}\right] + \frac{Ph}{kA}.T_a.\Delta x - \frac{Ph}{kA}T_P.\Delta x + \frac{\sigma.P}{kA}.\varepsilon.T_a^4.\Delta x - \frac{\sigma.P.\varepsilon}{kA}\Delta x[-3T_P^{*4} + 4T_P^{*3}.T_P] = 0 \tag{8}$$

Thus, rearranging eq. (8) may be written in the generalized discretization form given by eq. (9),

$$a_P T_P = a_e T_e + a_w T_w + b \tag{9}$$

Where,

$$a_P = \frac{2}{(\Delta x)^2} + \frac{Ph}{kA} + \frac{\sigma.P}{kA}\varepsilon.4T_P^{*3}$$

$$a_e = 1/(\Delta x)^2$$

$$a_w = 1/(\Delta x)^2$$

$$b = \frac{\sigma.P}{kA}\varepsilon.3.T_P^{*4} + \frac{Ph}{kA}T_a + \frac{\sigma.P}{kA}\varepsilon.T_a^{*4}$$

Boundary conditions

i) ó$T_b$ôis the same as the temperature of the metal base, which is identical to the ambient temperature óT_∞ô i.e. 300 K.

ii) The end of glass bore temperature is the one optimal for IR detector operation i.e. ‘T_d’ which is 77 K in the present case.

Thus, the boundary conditions are case of Drichlet boundary with fixed temperatures being specified at both the boundaries.

Working algorithm

The basic algorithm for solution of steady state cryochamber heat transfer problem is as under;

i) Define the input conditions; material properties, boundary conditions and geometry of the domain to be evaluated.

ii) Define the number of control volumes

iii) Discretize the equation and calculate the coefficient a_p, a_w , a_e , b from the input conditions for each control volume.

iv) Specify the applicable boundary conditions and calculate coefficients for boundary cells.

v) Solve the equations using standard Tridiagonal Matrix algorithm (TDMA) to generate the temperature field along the length of the cold well.

vi) Iterate for non linearity of the equation till convergence criterion of 1e-3 is met.

The code has been developed in *Matlab* adhering to the above stated algorithm.

3.0 Numerical Results

The present section is devoted to the presentation of parametric results of thermal modeling of cryochamber. The results for steady state thermal numerical analysis are discussed.

Tab. 1: Dimension and properties of glass cryochamber

Hollow glass cryochamber (Case-I)	
Outer diameter *(d_o)*	9.4 mm
Inner diameter *(d_i)*	7.2 mm
Length *(L)*	48 mm
Density *(ρ)*	2640 kgm^{-3}
Gas conduction coefficient *(h)*	1.0 $Wm^{-2}K^{-1}$ ($\equiv$ 0.9 Pa or 6.84 x 10^{-3} torr)
Cold well thermal conductivity *(k)*	0.8 $Wm^{-1}K^{-1}$
Cold well specific heat (C_p)	800 $Jkg^{-1}K^{-1}$
Emissivity *(ε)*	0.02
Base Temperature *(T_b)*	300 K
Detector temperature *(T_d)*	77 K

A typical glass cryochamber (Case-I) is considered having material and transport properties given Tab.1. The temperature profile along the length of the cryochamber is determined and is shown in fig (3). In order to check the efficacy of the numerical model developed the first task is to perform the grid independence check. The grid independence check is carried out by varying the no. of grids. In the present case the above problem has been solved employing 24 grids (size 2mm), 48 grids (size 1 mm) and 96 grids (size 0.5 mm) , and overlapping temperature profiles have been obtained, as shown in fig. 3. This proves that the profile is not changing with grid size and hence 48 grids have been typically used in the analysis.

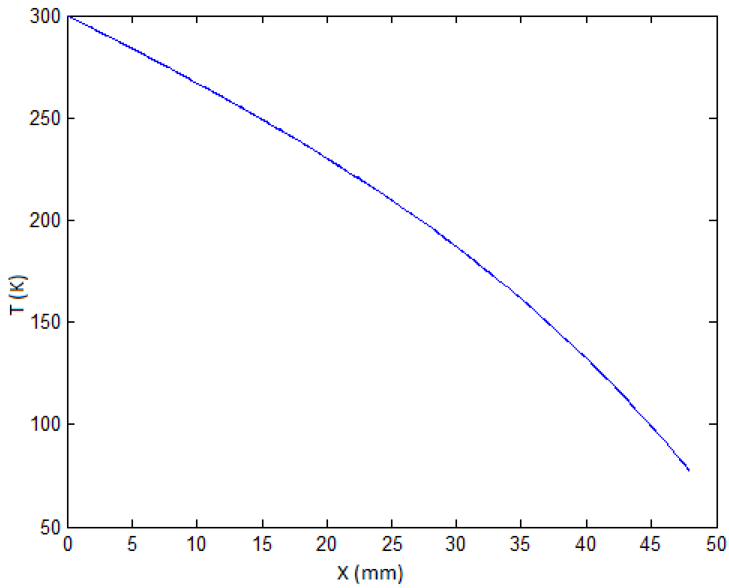

Fig. 3: Temperature profile along the length of the cryochamber
Three set of grids, 24, 48 and 96 have been used for grid independence study

Here, gas conduction coefficient *(h)* is a critical parameter and is determined from the theory of rarefied gas conduction [10] with our interest in low pressure regime of $5x10^{-3}$ to 2 torr. It is therefore, calculated using the following relations available in literature as function of pressure (P in Pa). Also, k_{air} thermal conductivity of air (14.8 x 10^{-3} $Wm^{-1}K^{-1}$) and D is the enclosing vessel diameter (19.4 mm for Case ï I and 20 mm for Case II)

$$h = 1.48P \quad for \quad P < P_{fm} \tag{10}$$

$$h = \frac{1.48P}{1 + 0.34P} \quad for \quad P_{fm} < P < 1 torr \tag{11}$$

$$h = \frac{2k_{air}}{d_o \ln(D/d_o)} = 4.35 \quad for \quad P > 1 torr \tag{12}$$

Where, P_{fm} is the pressure below which the free molecular gas conduction regime occurs and this limit is calculated considering that it occurs for cases where Knudsen number *(Kn)* [defined as ratio of free molecular mean free path *(λ)* to the characteristics dimension *(l_s)* (which is gap spacing in our case)] is greater than 10. It is given as,

$$P_{fm} = \frac{k_B T}{Kn\sqrt{2}\pi a^2 l_s} = \frac{k_B T}{10\sqrt{2}\pi a^2 l_s} \quad \textbf{(13)}$$

Here, *a* is the molecular diameter of air (0.37 nm). The first expression is general and the latter is considering Kn =10. Thus, considering average operating temperature between 77K and 300 K, the P_{fm} value turns out to be 2.72 x10^{-4} torr. The gas conduction coefficient is hence essentially a function of pressure inside the cryochamber, evident from eq. (10) to (12). In present case, eq. (11) has been used for calculating *h* and for simulating pressure higher than 1 torr *h* value has been taken as 4.35 (as shown in fig 4.) as cryochamber geometry is fixed.

After, establishing the effectiveness of the model a parametric analysis for the same geometry is done by varying the gas conduction coefficient *(h)*. The effect on temperature profile for various gas conduction coefficients has been shown in fig.4.

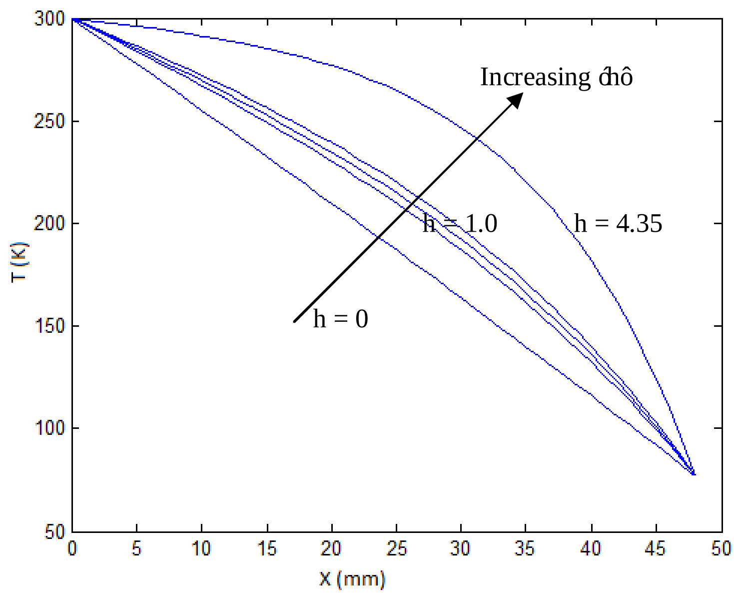

Fig. 4: Length profile of temperature for various gas conduction coefficients *h* = 0, 0.632, 0.8, 1.0, 4.35

Another, parameter that may vary owing to the extent of polishing of the cryochamber surface is the emissivity *(ε)*. Hence, the temperature profile has been generated by varying the emissivity and is shown in fig.5. It is apparent that the effect of emissivity variation on overall temperature profile is marginal since the contribution of radiation heat transfer as compared to gas and thermal conduction is relatively small.

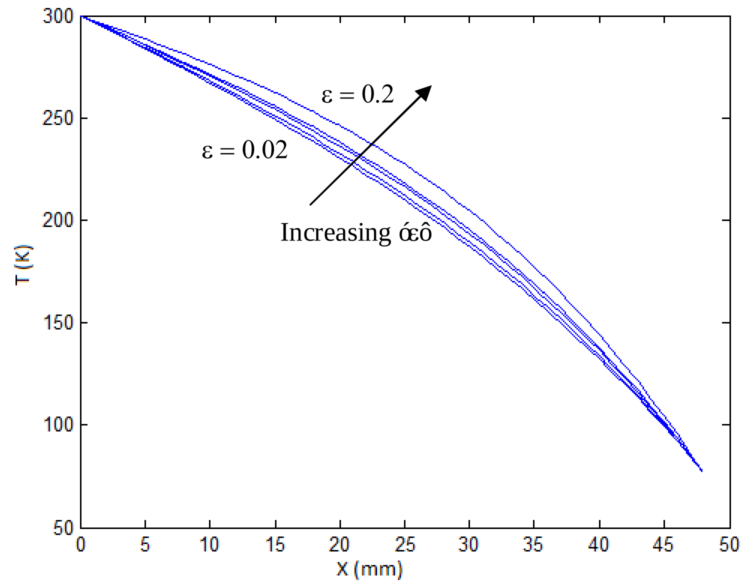

Fig. 5: Length profile of temperature for various emissivity's, ε = 0.02, 0.04, 0.08, 0.1, 0.2

Another case analyzed was for a hollow metal cryochamber (Caseï II), the typical material and transport properties considered are given in tab. (2).

Tab. 2: Dimension and properties of steel cryochamber

Hollow steel cryochamber (Case II)	
Outer diameter *(d_o)*	10.5 mm
Inner diameter *(d_i)*	10.3 mm
Length *(L)*	48 mm
Density *(ρ)*	7960 kgm^{-3}
Cold well Thermal conductivity *(k)*	1.2 $Wm^{-1}K^{-1}$
Cold well Specific heat (C_p)	500 $Jkg^{-1}K^{-1}$
Emissivity *(ε)*	0.074
Base Temperature *(T_b)*	300 K
Detector temperature *(T_d)*	77 K

The effect of variation in heat conduction coefficient has also been studied. The results are shown in fig. 6 for gas conduction coefficient varying between ό0ô to ό4.35ô. A comparative analysis of the profiles of glass and steel cryochamber reveal that the temperature profile is much steeper in case of steel than in case of glass. It is understandable, since the major portion of heat transfer is through thermal conduction, and steel has sufficiently larger thermal conductivity as compared to that of glass.

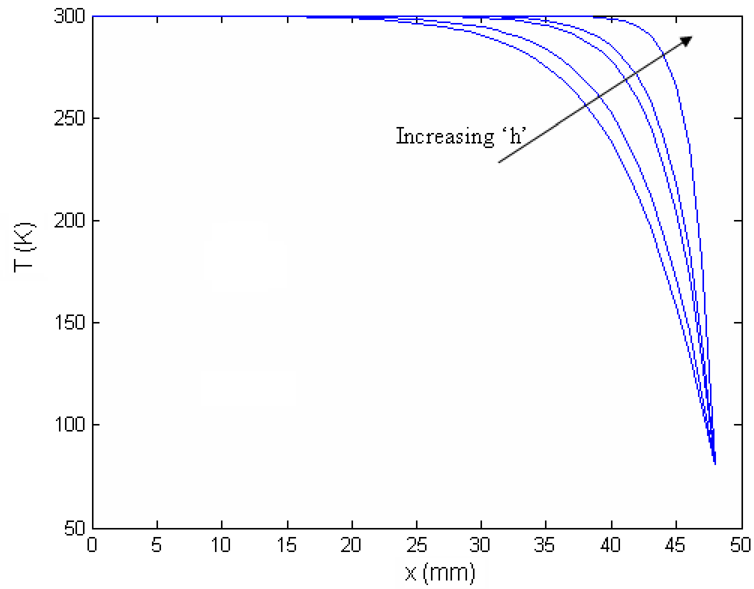

Fig. 6: Length profile of temperature for various gas conduction coefficients,
***h* = 0, 0.632, 0.8, 1.0, 4.35**

5.0 Validation

The validation studies for the developed numerical model were carried out by performing experimental thermal testing of IR cryochamber. The schematic and configuration of the experimental set up used for the cryochamber experiments for validation of the simulation results is shown in fig. 7.

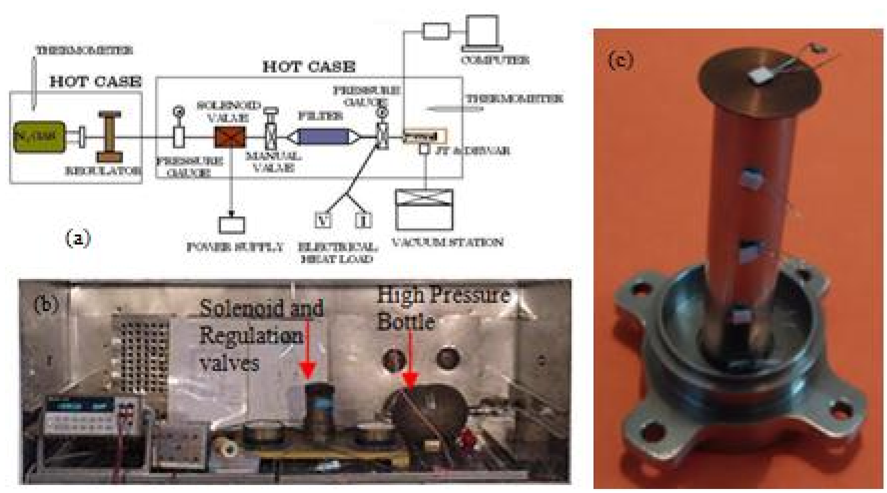

Fig. 7: Experimental setup; (a) Schematic, (b) Photograph, (c) 5 RTD mounted on cold well

The main components are; cryochamber assembly with Joule-Thompson cooling provision, high pressure bottle, solenoid and regulation valves and the filter assembly connected to data acquisition. Five numbers of RTD (Resistance Temperature Device), type Pt-100 (Make: Omega, Model: PR-17) were mounted at, x = 0 mm, 12 mm, 24 mm, 36 mm, 48 mm on the cryochamber surface (shown in fig. 7) for determining the temperature profile along the length of the cryochamber under steady state condition.

The results for glass cryochamber are shown in fig. 8. The effect of variation of gas conduction coefficient on account of change in cryochamber pressure was studied for twin pressures of 0.9 Pa and 140 Pa for cryochamber surface emissivity *(ε)* of 0.02. The obtained experimental and numerical temperature profiles are also shown for comparison. It is evident that the experimental data is in close agreement with the numerically predicted profile. The maximum variation of nearly 9 % occurs close to the maximum gradient region.

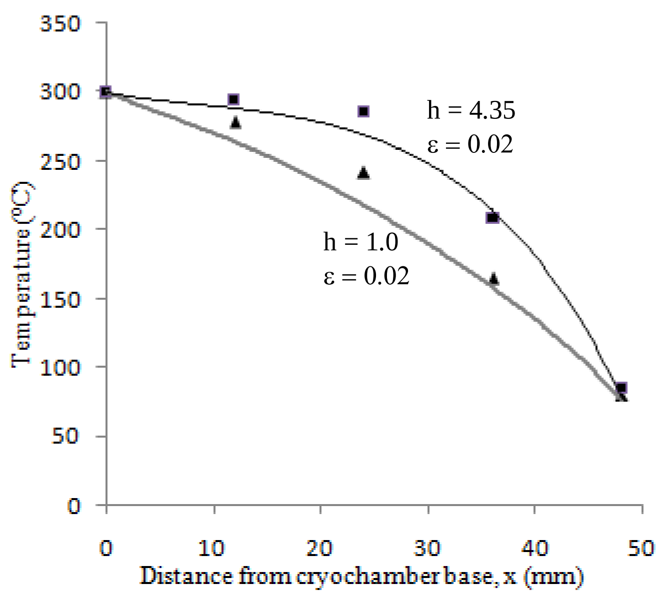

Fig. 8: Length profile of temperature for glass cryochamber for gas conduction coefficient, h = 1.0, 4.35; emissivity, ε = 0.02, Numerical (Line), Experimental (Data point)

Similarly, the experimental data for the case of metallic chamber is shown in fig. 9. The experimental data compares reasonably well in qualitative terms with the numerical data (shown in fig. 6), showing a steep fall in temperature owing to high thermal conductivity of material of construction.

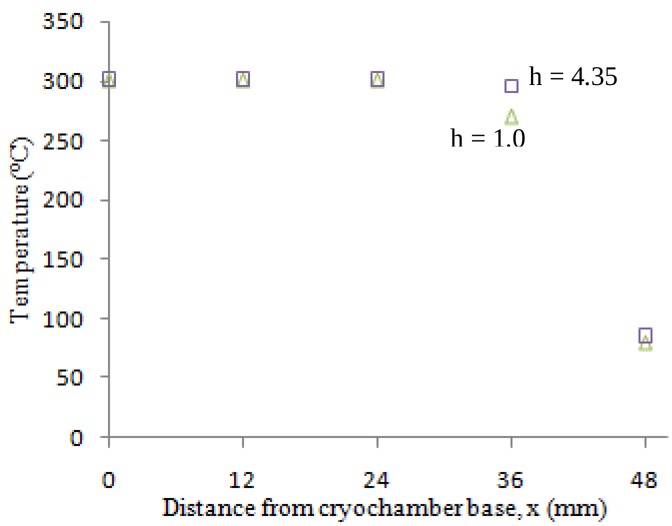

Fig. 9: Experimental length profile of temperature for metallic cryochamber for gas conduction coefficient, h = 1.0, 4.35; emissivity, ε = 0.074

Similarly, the experimental data for the case of metallic chamber is shown in fig. 9. The experimental data compares reasonably well in qualitative terms with the numerical data (shown in fig. 6), showing a steep fall in temperature owing to high thermal conductivity of material of construction.

However, it is evident that in order to accurately capture the steep change in temperature quantitatively along metallic cryochamber several more temperature sensing elements will be required. Due to practical constraints of proper mounting and corresponding feed through it was practically not feasible to mount additional such elements in the present system.

6.0 Conclusions

A suitable numerical model for performing thermal analysis of IR cryochamber has been presented. The effects of variation in cryochamber material, gas conduction coefficient (which in turn is a function of gas pressure), emissivity on thermal behavior are discussed. The model has been validated experimentally to prove its efficacy. It may be safely concluded that gas conduction coefficient greatly influences the temperature profile of the cryochamber whereas emissivity has only a marginal effect on the same. The cryochamber made of glass as the material of construction encounters a more gradual variation of temperature along the length for all heat conduction coefficients whereas for a steel cryochamber the temperature variation is quite steep.

[1] Tidrow, M.Z., Dyer, W.R. ñInfrared sensors for ballistic missile defenseò Infrared Physics and Technologyò, 42 (2001), pp 333-336

[2] Matthews, S., *Thermal Imaging on the rise,* Laser Focus World, Janó2004.

[3] Kang, B.H., Lee, J.H., Kim, H.Y., An experimental study on the cooling characteristics of an Infrared detector cryochamber, *Korean Journal of Air- conditions and Refrigeration Engineering*, 2004, Vol. 16

(10), pp. 889-894.
[4] Kim, Y.M., Kang, B.H., Thermal analysis of a cryochamber for an infrared detector considering a Radiation shield, *Korean Journal of Air- conditions and Refrigeration Engineering*, 2006, Vol.18 (8), pp. 672-677.
[5]Kim, Y.M., Kang, B.H., Park, S.J., An experimental study on the thermal load of a cryochamber with Radiation shields, *Korean Journal of Air- conditions and Refrigeration Engineering*, 2008, Vol. 20 (1), pp. 11-16.
[6] Mills, A.F., *Heat Transfer*. Concord (MA), Irwin, 1992.
[7] Koschmieder, E. L., *Bénard Cells and Taylor Vortices*. Cambridge, ISBN 0521-40204-2, 1993.
[8] Golmski, M., Johnson, A.M., A precise calculation of critical Rayleigh Number and Wave Number for the Rigid-Free Rayleigh- Benard Problem, *Applied Mathematical Sciences*, 2012, Vol. 6, pp. 5097-5108
[9] Herring, J.R., Investigation of problems in Thermal Convection: Rigid Boundaries, *Journal of Atmospheric Sciences*, 1964, Vol. 21, pp. 277-290.
[10] Springer G. S., Heat Transfer in rarefied gases. Advanced Heat Transfer, 1970, Vol. 7, pp. 163-218.
[11] Patankar, S.V., *Numerical Heat Transfer and Fluid flow*, Hemisphere, New York, 1980.